Environmental and Climate Technologies
2024, vol. 28, no. 1, pp. 94–106
https://doi.org/10.2478/rtuect-2024-0009
https://content.sciendo.com

Hydrothermal Conversion of Fly Ash into Monomineralic Zeolite Synthesis for Biodiesel Production

Maria K. KOCHANIEC[1*], Ewelina GRABIAS-BLICHARZ[2], Wojciech FRANUS[3]

[1]*Faculty of Chemistry, Warsaw University of Technology, Noakowskiego 3, 00-664 Warsaw, Poland*
[2]*Department of Analytical Chemistry, Medical University of Lublin, Chodźki 4A, Lublin, 20-093, Poland*
[3]*Faculty of Civil Engineering and Architecture, Department of Construction Materials Engineering and Geoengineering, Lublin University of Technology, 40 Nadbystrzycka St., 20-618 Lublin, Poland*

Received 02.06.2023; accepted 23.01.2024

***Abstract* – Fly ashes as a residue from combustion processes of coal in coal-fired power stations can be applied for zeolite formation. The zeolite synthesis has considerable effect on their structure following further catalytic use. The formation of analcime is guided by the operation of the silicate framework in the company of Na^+, $[Al(OH)_4]^-$, $[H_2SiO_4]^{2-}$ species, coming from fly ash processing. Here, we have highlighted the importance of conducting the coal fly ash waste management towards monomineralic zeolite synthesis, in the form of powder analcime. It is the first report on powder analcime production without fly ash residues, confirmed by SEM and XRD analysis. The obtained analcime-zeolite was further explored as biodiesel catalyst based on base-catalyzed transesterification process. The effect of analcime catalyst usage on the biodiesel yield was determined with observed 97.2 % conversion efficiency under the concentration of 4%wt at 230 °C, with three times reusable analcime catalysts. Coal fly ash-derived monominerals on a large scale can significantly contribute to the sustainability goals and efficient waste management.**

***Keywords* – Analcime; biodiesel; fly ash management; powder aggregates; monominerals; powder zeolite.**

Nomenclature		
CFA	Coal fly ash	–
SEM	Scanning Electron Microscope	–
XRD	X-ray diffraction	–
ANA	Analcime	–
FAME	Fatty acid methyl esters	–
LOI	Loss on ignition	–
HIC	High carbon fly ash	–
XRF	X-ray fluorescence	–
GC-MS	Gas Chromatography-Mass Spectrometry	–

* Corresponding author.
E-mail address: maria.kochaniec@pw.edu.pl

©2024 Author(s). This is an open access article licensed under the Creative Commons Attribution License (http://creativecommons.org/licenses/by/4.0).

1. INTRODUCTION

There is no simple way for overcoming the negative implications of the current coal fly ash (CFA) waste generation. CFA as a waste of thermal power stations is one of the main fears to the ecosystem and human well-being. The United States Environmental Protection Agency categorized CFA like a non-hazardous waste while their reports revealed in 2020 stated that over 90 % of CFA impoundments are polluting nearby surface and groundwater sources [1]. In spite of the regulations which do not require companies to move the CFA out of the unlined pits the hazard awareness have forced society to seek advanced CFA waste management. Nevertheless, the use of cheap Si and Al sources from CFA may be considered as a low-cost feedstock for zeolite synthesis. The well-established procedure involves alkali fusion from CFA followed by hydrothermal treatment to achieve a desired X-type zeolite structure [2]. For instance, the conversion of Indonesian zeolite into analcime (ANA) form was conducted under hot-water conditions [3] leading to zeolites with high crystallinity. Sandoval *et al.* suggest that ANA can be manufactured from natural clinker [4]. Indeed, ANA minerals occur in limited regions around the globe, thus the synthetic methods are the most common sources for the artificial synthesis. Up to date, ANA was primarily created out of substances like glass and aluminium. Kaolin as a clay and the most used phyllosilicate for the zeolites synthesis was already reported for ANA synthesis [5]. ANA zeolite exhibits the smallest-pore zeolite with a uniformed unit cell of $Na_{16}Al_{16}Si_{32}O_{96} \times 16H_2O$. ANA is nowadays an important module in dental porcelains [6], heterogeneous catalysis [7], [8], agriculture (fertilizer dispenser) [9] and adsorptions [10]. ANA synthesis protocols rely mostly on silica-rich kaolinite rock calcination followed by hydrothermal treatment [5]. Rice husk ash coupled with kaolin are aluminosilicate minerals for ANA production [11]. Hydrothermal treatment of ANA together with hydroxycancrinite reported that the decline of sodium metasilicate merger owed the ANA product. The synthesis of ANA is a boundary attached to dissolving-reprecipitation procedure occurring in the silicate structure [12].

The three-dimensional frameworks of SiO_4 and AlO_4 tetrahedra are specified to form zeolites in the channels containing water and exchangeable cations. In the ANA system of SiO_4-AlO_4 tetrahedrons dominate, forming a 4-membered ring, which combine into 6- and 8-membered rings. The arrangement of structural units causes the formation of inner holes of the crystal form with dimensions of 2.6×2.6 Å, according to the International Zeolite Association sources [13]. By controlling the crystal polymorphic production of Na-zeolites the crystal arrangement and assets can be customized with no foregoing crystal level cleanliness [14]. Indeed, plenty of zeolites can be applied in catalysis and adsorption in the environment [15]. Zeolite made from hydrothermal response of natural diatoms in NaOH environment can serve as transesterification catalyst [16].

Biodiesel production seems to be real alternative in order to enhance the engine performance coupled with emissions level by applying the third-generation biofuels and its blends [17]. Biodiesel offers sustainable solution derived from animal fats and vegetable oils. It replaces diesel in the compression ignition (CI) engine. From chemical point of view, the biodiesel is classified as mono-alkyl esters of long fatty acids received through transesterification or esterification catalytic reactions. Biodiesel needs to meet the requirements and conditions underlined in the specifications ASTM D6751 & EN 14214 [18]. Heterogeneous acid catalysts show good recyclability since they can be reused after the biodiesel production. Through improved susceptibility to fatty free acids and the water, it is recommended to keep a high-level basic power of zeolitic-based catalysts [19]. The eggshell-moringa leaf composite catalyst was already applied with high activity reaching 94.3 % of fatty acid methyl esters (FAME) [20]. Beneath enhanced reaction restrictions:

proportion of ethanol to oil of 15:1 M with 10 wt.% of catalyst loading, and a reaction temperature of 70 °C designed for 50 min the yield in the range of 84.6 % FAME was detected. Doyle and co-workers examined the acid catalytic performance of zeolite Y, in the esterifying of oleic acid. The best transformation received with help of zeolite catalyst was 85 % with the ratio of 6 M ethanol/1 M oleic acid, and with 5 wt.% of catalyst use for 1 h [21].

In this work, for the first time, we have successfully produced from CFA, the pure powder ANA zeolite catalysts for biodiesel production which revealed monomineralic zeolitic phase composition. The Si and Al sources used were the post-reaction solutions after conversion of CFA on the semi-technical scale to zeolite manufacturing. Through varying the synthesis temperature, the waste solution and NaOH ratios we have established the synthesis protocols for ANA production and their composition with the raw fly ash characterized by high unburned carbon content (HIC). HIC is named as off-spec CFA which do not meet the physicochemical criteria outlined in ASTM C618, where the upper limit of loss on ignition (LOI) of FA is 6 %, while the European Standard (UNI-EN 206) sets out to a LOI of 5 %. Overall, the aim of this article was an attempt to use for the first time, a monomineral zeolite phase (analcime), obtained from a waste solution after the conversion of fly ash to zeolite, as a catalyst for the production of biodiesel derived from used cooking oil. The use of coal combustion waste (fly ash) for the production of catalyst (analcime), and at the same time the production of biodiesel from the used cooking oil are in line with sustainable development goals and reduce the amount of unutilized industrial and domestic waste. Reuse and recycling can also reduce the environmental effects of coal production. Obviously, it will not decrease the emissions from coal-fired power plants. However, some promising application of materials obtained from fly ash are adsorbents, for example as CO_2 adsorbents.

2. Materials and Methods

2.1. Formulation of ANA compound

The aqueous solution of 2M NaOH (25 mL) and the source of aluminium in the form of 1 g of aluminium scotch (>99 % Al, Pol-Aura, Zabrze, Poland) has been employed to reach the relevant Si/Al relation in the synthesis protocol. All chemicals were mixed and added to the 50 mL of post-reaction solutions, applying a technical line depicted by Wdowin *et al.* [22] and built on the basis of the PL224734B1 polish patent, where the chemical composition was the following: Na (19 mg/L), Si (14 mg/L), Al (36 mg/L) [23]. All ingredients have been left in a glass inlet hermetically sealed in a Teflon autoclave and kept at 180 °C for 24 h (p ~10 bar). The solid precipitate remained to rinse for several times with distilled water until the leak achieved the pH 8, following by filtering and drying at 105 °C for 24 h, leading to the formation of ANA3. ANA2 was prepared at 200 °C while ANA1 stand from 25 mL of 1 M NaOH used as substrate and heated up to 180 °C, respectively. ANA samples were gathered and stored in desiccator before further investigation.

2.2. Preparation of HIC and HIC-derived zeolites

HIC was sourced from the Janikowo Heat Power Plant (Janikowo, Poland). To increase the accessibility of the reactive fly ash components, HIC was subjected to milling in a ball mill (Pulverisette-5, Fritsch, Germany) for 3 h. Then, milled powder HIC was used to obtain HIC-derived zeolites according to the procedures given in section 2.1., in which 5 g of milled HIC was added to the given substrates (marked as ANA3 in the section 2.1.) and the products obtained were designated as HIC-ANA.

2.3. Characterization Methods

Post-reaction liquid configuration was defined by means of Inductively coupled plasma mass spectrometry (ICP-MS) by Agilent 8900 Triple Quadrupole apparatus. Determination of the chemical structure was performed by semi-quantitative energy dispersive X-ray fluorescence (ED-XRF) method on Epsilon 3× apparatus. The mineral arrangement of zeolites was assessed by X'pert MPD X-ray diffractometer with Cu lamp and a graphite monochromator registered with a step size of 0.02°. The morphology was then examined employing FEI Quanta 250 FEG Scanning Electron Microscope (SEM). FT-IR/DRS spectrum were retrieved at the range of 4000–400 cm^{-1} with resolution of 4 cm^{-1}, mirror speed of 2.5 kHz and 1024 interferogram scans. Biodiesel viscosity was investigated using the Ostwald viscosimeter.

2.4. Biodiesel production and yield

The used cooking oil in the amount of 200 mL was filtered and mixed with 25%wt of methanol and 4%wt of ANA followed by the esterification-transesterification process. The reactor was heated up to a temperature of 180 and 230 °C, respectively and maintained for one hour once the reached temperature. The biodiesel was examined employing Gas Chromatography-Mass Spectrometry (Trace GC Ultra PolarisQ – Thermo). The yield was calculated as the ratio of the product obtained and the raw material used here.

$$\text{Yield of biodiesel} = \frac{\text{weight of biodiesel}\left[\text{g}\right]}{\text{weight of feed}\left[\text{g}\right]}$$

2.5. Biodiesel density

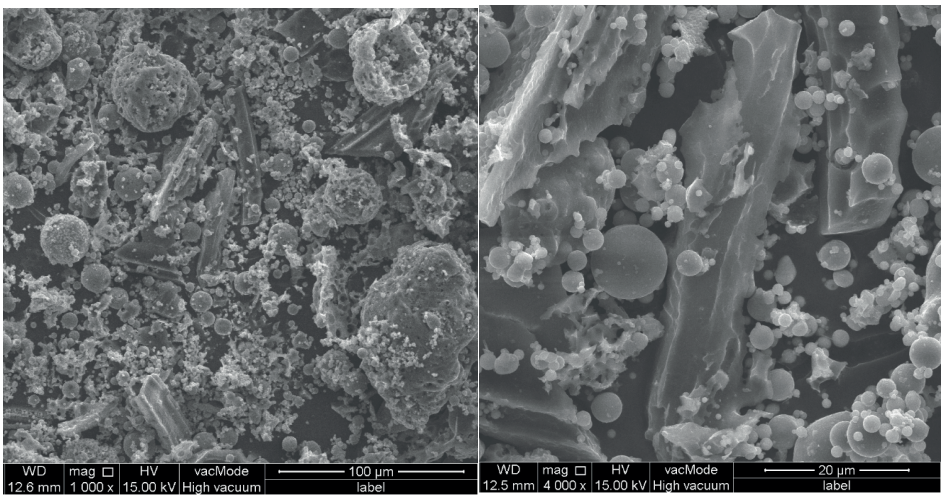
By weighing the empty pycnometer (wb) with the volume V and the pycnometer containing biodiesel (w0), the density was calculated by the following formula:

$$\text{Density}\,\rho = \frac{\text{w0} - \text{wb}\left[\text{g}\right]}{\text{V}\left[\text{mL}\right]}.$$

3. RESULTS AND DISCUSSION

3.1. Description of zeolites

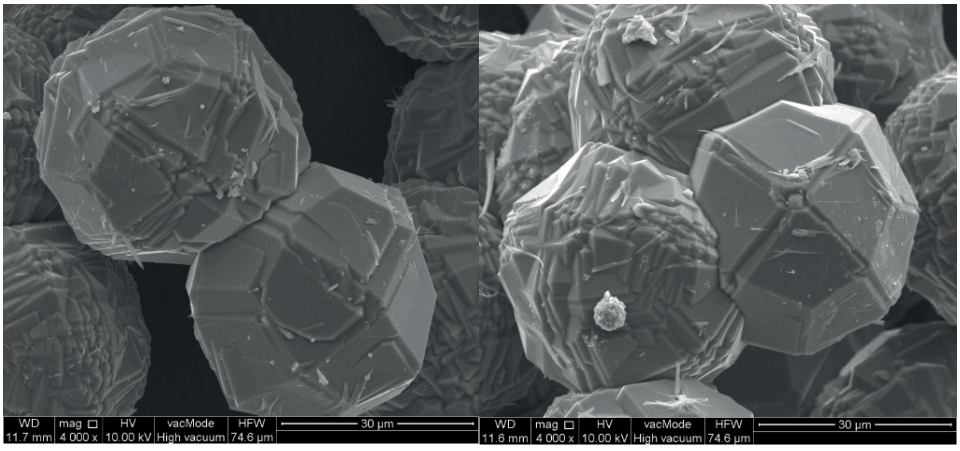
Powder HIC contains mostly silicon, aluminium and iron oxides. The morphology of the HIC is presented in Fig. 1. SEM pictures indicate that grains of HIC fly ash consist of irregular quartz and mullite particles, spherical amorphous aluminosilicate glaze, small amounts of hematite, as well as fractions of organic carbon. Milling, for a contrary, resulted in the fragmentation of powder HIC particles into a finer fraction, which increases the reactivity and availability of reactive HIC components in the HIC conversion reaction with NaOH and post-reaction solutions [24]. The mineral composition of the HIC shows reflections characteristic of quartz (Q according to The International Centre for Diffraction Data (ICDD) No. 01-075-8320), mullite (M) ICDD 01-074-4145) and haematite (M) ICDD 39-1346. Furthermore, a characteristic hump confirming the amorphous phase is also prominent in a wide range of 12–32° 2θ (Fig. 4).



(a) (b)

Fig. 1. SEM pictures of powder HIC (magnification a) 1000× and b) 4000×).

The morphology of the synthesized zeolitic materials were visualized by SEM (Fig. 2). It leads a typical maximum length of the crystal is observed to be across 50–70 µm while for the HIC-ANA composites the crystals reached above 100 µm. The ANA crystal satisfies when contrasted with the dimension of the minerals obtained through kaolinite leaching by other scientists. Jamil *et al.* [25] produced ANA from kaolinite with an average crystal size of 5–7 µm, whilst ANA grains obtained by Hegazy *et al.* reached up to 10 µm [26]. More recently, Novembre and Gimeno reported ANA crystals with dimensions up to 25 µm [5].



(a) (b)

Fig. 2. (a-b) SEM representations of the manufactured ANA (magnification 4000×), and (c-d) HIC-ANA (magnification 4000× and 2000×, respectively).

Particle size distribution and percentage share (%) of grain fractions of ANA zeolites are presented in Fig. 3 and Table S1. The ANA zeolites obtained are of various particle size distributions. The ANA1 sample represents a bimodal particle distribution with majority of

grains in the 100–250 μm and 2–20 μm ranges (32.7 % and 19.49 %, respectively). Moreover, fractions in the 20–50 μm and 50–100 μm range account for about 33 %.

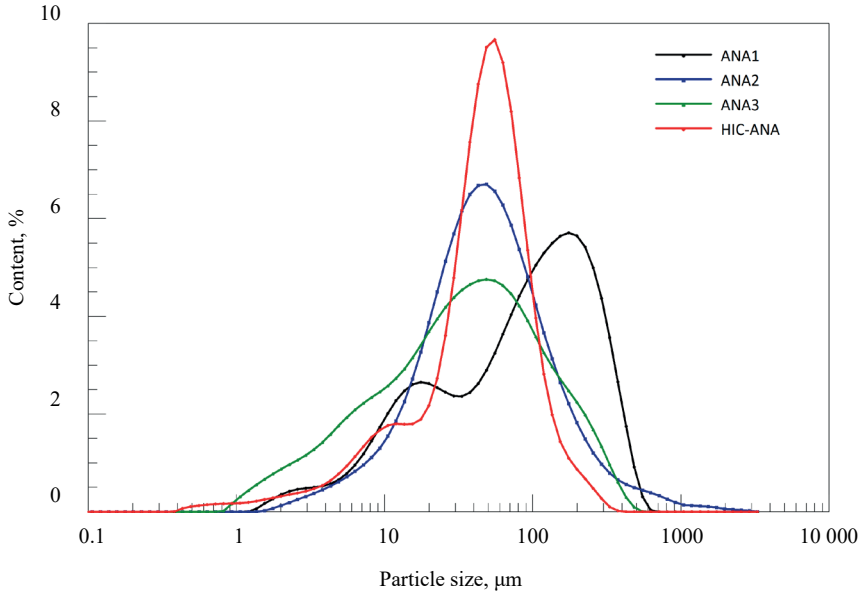


Fig. 3. Particle size distribution of ANA and HIC-ANA samples.

Particles no larger than 285 m account for up to 90 % of all granules present in ANA1 (Dx (90)) (Table S1), whereas the value of the median particle size is 90.4 μm (Dx (50)). In the brief case of sample ANA2 and ANA3, we can notice a broad monomodal distribution with tailing for sample ANA3. For both samples, particles of size no more than 169 μm and 161 μm (for ANA2 and ANA3) account for up to 90 %. The amount of the median particle size (Dx (50)) is 47.3 μm and 35.7 for ANA2 and ANA3, respectively (Table S2). In contrast, a narrow and predominantly monomodal particle distribution is obtained for the HIC-ANA sample. According to Bandura *et al.* [27] HIC which was the precursor for obtaining HIC-ANA zeolite, represents an average particle size of 65.8 μm. However, the HIC-ANA sample is dominated by fractions in the range of 20–50 μm and 50–100 μm (34.57 % and 35.56 %), with typical particle size of 47.2 μm (Dx (50)). Conversely, 90 % of the particles are no larger than 103 μm. Nevertheless, by manufacturing zeolites a theoretical framework has been established for the impact of grain distribution [28]. The XRD diffractograms of ANA and its pattern are described in Fig. 4. Reflections of well crystallized ANA have been examined with no CFA residue. Characteristic reflexes were identified for ANA, among others with the corresponding interplanar spacing, dhkl values = 5.60, 4.85, 3.67, 3.43, 2.925, 2.69 and 2.50 Å. No other reflexes, apart from ANA phases, were identified in the samples ANA1 and ANA3. The ANA3 was distinguished by monomineral zeolitic phases of high purity and the XRD outcomes are in line with the diffractograms of trade ANA confirming that post-reaction solution can be successfully converted into ultrapure zeolites sources. The desired shape, altitude, and reflective pattern of the diffractograms and their marketable equivalents prove the superior level of the crystallization of the, as obtained for ANA3 catalysts. Other reflexes, as the minority were assessed as cancrinite phases which come from high temperature treatment (ANA2). Built on the pattern and the use of correspond software program, the highest peak intensities of the manufactured zeolites were observed at 15.977, 26.123, and

30.717° indicating the tetragonal crystal system of ANA ($Al_{1.9}Na_{1.86}O_{12}Si_4$) and trace cancrinite contents diffraction patterns (ICDD No. 00-044-01030 and 01-075-5322, respectively).

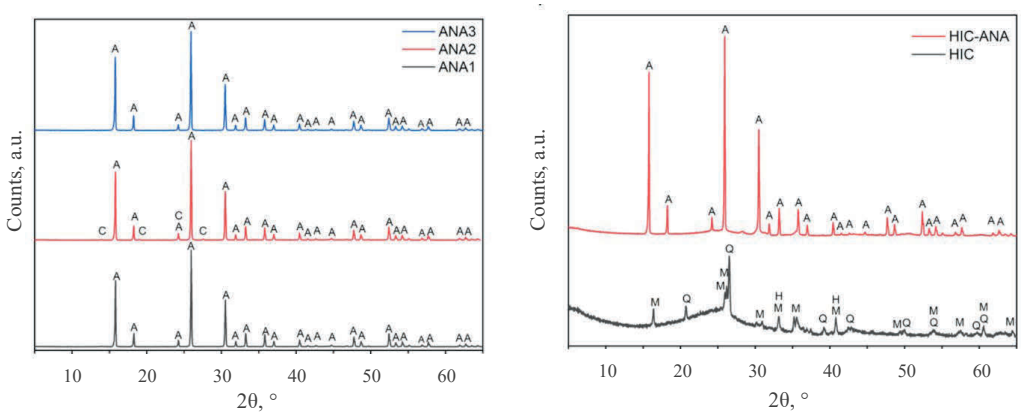


Fig. 4. XRD patterns of pure ANA zeolites (a) and ANA-HIC zeolite, HIC samples (b).

In order to estimate the quantifiable content (% of crystallinity), the summation of the areas of the seven key diffraction reflections was indicated [24]. Then, the largest calculated area was assumed to be the reference corresponding to 100 % crystallinity. For the remaining samples, the determined sums of peak areas were divided by the reference and their % crystallinity was calculated. The ANA3 sample appeared to represent 100 % crystallinity. HIC-ANA was then prepared from the procedure used to obtain the ANA3 sample, which, despite being obtained based on waste fly ash (HIC), is characterized by nearly 50% crystallinity (Table S3). Zhang *et al.*, have demonstrated that high crystallization temperature outcomes in hydroxylsodalite while low SiO_2/Al_2O_3 fostered shaping of crystals with larger mean grain dimensions [29]. The elemental composition of HIC and the synthesized ANA samples have been analysed using XRF showing the corresponding results. HIC is an off-grade fly ash, with a carbon content of almost 38 %, and its chemical composition is as follows (Table 1).

TABLE 1. XRF ANALYSIS FOR HIC, ZEOLITES AND ZEOLITES-DERIVED HYBRIDS

Component	HIC	ANA3	HIC-ANA
	Weight percentage, %		
Na_2O	0.52	9.50	6.23
MgO	1.47	0.62	2.46
Al_2O_3	13.23	12.49	8.67
SiO_2	28.50	71.57	32.58
P_2O_5	0.34	0.06	0.41
SO_3	1.57	0.24	0.57
K_2O	2.33	1.50	1.19
CaO	4.32	0.79	5.10
TiO_2	1.32	0.23	1.55
Fe_2O_3	8.51	2.05	9.82
LOI	37.67	0.95	30.84

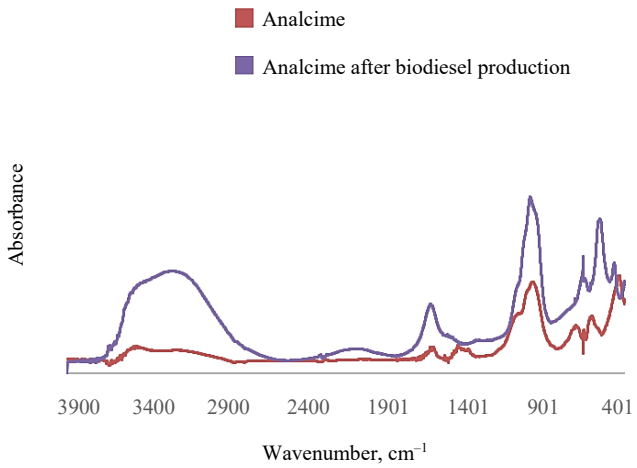


Fig. 5. FT-IR spectrum of investigated powder ANA3 sample.

It can be concluded that ANA3 contains the SiO_2, Al_2O_3 and Na_2O as the major components. The Na_2O content was 9.50 % due to the sodium hydroxide usage throughout the hydrothermal treatment.as a main chemical reagent during the synthesis. The concentrations of other oxides like K_2O and TiO_2 were at the trace levels.

Many studies have concluded so far that the conversion to esters depends on the methanol-to-oil ratios and with the optimal 4%wt of zeolite catalyst's dosage [30]. The catalysts used can be recycled, maintaining its stability and reactivity. The regenerated catalysts, after 2 hours of calcination procedure was further reused. However, an appreciable decrease is observed in biodiesel yield, reaching 78 % and 62 % for the second and third cycles, respectively. This phenomenon is widely described in the literature due to the diminished responsiveness or capability of the zeolites in the loss of active sites. The other reason is also a small surface area (up to 3.8 m^2/g) of zeolitic catalyst [31] which can be further blocked by oleic components. Nevertheless, the decrease in the conversion rate coupled with obvious leaching processes should lead to the reactivity studies of catalyst after regeneration. Figure 5 indicates the FT-IR spectrum of explored zeolites: the as synthesized and after biodiesel production (3-times used). The major broad peaks are situated at 3300 and 1640 cm^{-1} for O–H stretching and bending, correspondingly. Notably, the broad band at 3300–3400 cm^{-1} is correlated to an asymmetrical stretching mode of water coordinated to the edges of the canals. The band at 1640 cm^{-1} is attributed to the zeolitic water in the canals [32]. The bands at 1000 and 1030 cm^{-1} are allocated to stretching mode of O–Na–O, while the bands cantered at 714 and 625 cm^{-1} belong to the Si–O–Si symmetric stretching vibration seen in 4-membered rings. O–Si–O bonding mode are observed as bands at 446 and 416 cm^{-1} [33].

3.2. Characterization of the biodiesel

The results from GC-MS confirms the transformation of waste cooking oil to biodiesel (Table S4, Table S5). The results of the GC-MS analysis showing the difference in fatty acid esters in the essay. Due to the high crystallinity leading to the highest conversion yield the GC-MS for biodiesel product was performed specifically for the ANA3 samples with the best biodiesel yield.

It is well known that the waste cooking oil has the capacity as a feedstock to produce biodiesel once the correct catalyst is deserved. In this study the used cooking oil was characterized with density and viscosity of 974 kg/m^3 and 30.1921 mm^2/s, correspondingly. Biodiesel manufacturing relies on esterification–transesterification process using a zeolite catalyst, where dispersion appearing in the micro-zones of zeolite crystals (e.g., surface flow, diffusion anisotropic characteristics, and limited diffusion) affect underlying response system, catalytic operations [34]. Table S6 provides the biodiesel content with its corresponding yields of methyl esters of 89.1 % and 97.2 % for biodiesel 180 and 230 °C, respectively. The separation was accelerated by flow centrifugation. The results of the GC-MS analysis (Table S4, Table S5) indicate the variations in fatty acid structure. The characteristics of used cooking oil include 9-octadecanoic acid and 9,12-octadecanoic acid as the major acids. The most dominant FAME were the acids: oleic (9Z-octadecenoic acid, methyl ester), linoleic (9Z,12Z-octadecadienoic acid, methyl ester) as well as palmitic (hexadecanoic acid, methyl ester). The data meet requirements of EN 14214 standard B for biofuels. Density and viscosity of the biodiesel generated from the esterifying–transesterification process were assessed and are given in the Table S7.

3.3. Biodiesel production mechanism

During the esterification–transesterification reaction, simultaneous fat hydrolysis and esterification of fatty acids by methanol take place. The chemical composition of ANA3 and their derivatives is based on base-catalyzed transesterification process. The, as introduced NaOH solution consequences in the Si–O–Na groups formation [35]. Once, the methanol absorbs the surface of solid base, the active site – intermediate- of CH3O– is becoming prone to the nucleophilic attack on the carbonyl side of carbon next to triglyceride (Fig. 6). The rearrangement forms the FAME, following the deprotonation of the active site of Broensted base abstracting hydrogen out of methanol called as the deprotonation of alcohol [31], [36]. Monoglyceride interacts with active nucleophile leading one mole of fatty acid methyl ester and glycerol as undesired consequence [37]. Once the biodiesel is produced, the mixture self-separates where biodiesel is the lighter hydrophobic fraction [38], while the lower, heavier hydrophilic fraction contains glycerol and ANA catalyst. So far, heterogeneous catalyst were assessed by experimental studies and theoretical modelling underlying their importance in biodiesel production from waste cooking oil [39]–[41].

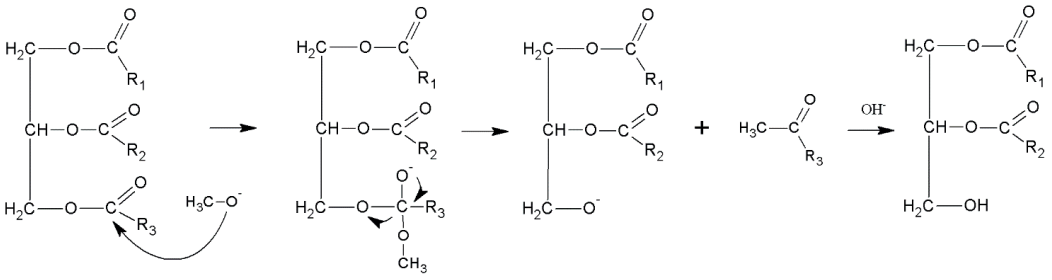


Fig. 6. Schematic mechanism of biodiesel production.

4. CONCLUSION

We successfully obtained zeolite type analcime from waste solution and waste fly ash with high carbon content. The formation of analcime is guided by the operation of the silicate framework in the company of Na^+, $[Al(OH)_4]^-$, $[H_2SiO_4]^{2-}$ species, coming from fly ash processing. The synthesis conditions may affect the counter ions affinity. Zeolites possess some affinity to adsorb selected ions as oxoanionic species. To the best of our knowledge, this is the first description of powder analcime production without fly ash residues, confirmed by SEM and XRD analysis. The obtained zeolite contained no ash residue with an average particle size of 30–50 μm. The used analcime biodiesel catalyst based on base-catalyzed transesterification process with altered rings and holes taken over by the Na ions generates an octahedral-coordination platform. The rearrangement forms the FAME, following the deprotonation of the active site of analcime. The most dominant FAME were the acids: oleic, linoleic and palmitic. The obtained contents of FAME meet requirements of EN 14214 standard for biofuels being prominent for oleic acid transformation in the third generation biofuels and its blends. The zeolite base-catalyzed transesterification holds severe advantageous such as environmentally benign, noncorrosive, recyclable, ease separation of products, longer catalyst life. Nevertheless, some limitations appear in terms of soap formation due the presence of high water contents and fatty free acids in the feedstock, and the produced FAME separation from glycerol.

ACKNOWLEDGEMENT

This work has been supported by the TEAM-NET programme of the Foundation for Polish Science co-financed by the European Union under the European Regional Development Fund, grant number POIR.04.04.00-00-14E6/18-00, 'The fly ash as the precursors of functionalized materials for applications in environmental engineering, civil engineering and agriculture'. Dr. Rafał Panek (Lublin University of Technology) is acknowledged for retrieving the SEM images of the samples.

REFERENCES

[1] https://nepis.epa.gov, accessed on January 7, 2024
[2] Murayama N., Yamamoto H., Shibata J. Mechanism of zeolite synthesis from coal fly ash by alkali hydrothermal reaction. *Int J Miner Process* 2002:64:1–17. https://doi.org/10.1016/S0301-7516(01)00046-1
[3] Lestari W. W., Hasanah D. N., Putra R., Mukti R. R., Nugrahaningtyas K. D. Transformation of Indonesian Natural Zeolite into Analcime Phase under Hydrothermal Condition. *IOP Conf Ser Mater Sci Eng* 2018:349:012068. https://doi.org/10.1088/1757-899X/349/1/012068
[4] Sandoval M. V., Henao J. A., Ríos C. A., Williams C. D., Apperley D. C. Synthesis and characterization of zeotype ANA framework by hydrothermal reaction of natural clinker. *Fuel* 2009:88(2):272–281. https://doi.org/10.1016/j.fuel.2008.08.017
[5] Novembre D., Gimeno D. Synthesis and characterization of analcime (ANA) zeolite using a kaolinitic rock. *Sci Rep* 2021:11:13373. https://doi.org/10.1038/s41598-021-92862-0
[6] Rasmussen S. T., Groh C. L., O'Brien W. J. Stress induced phase transformation of a cesium stabilized leucite porcelain and associated properties. *Dent Mater* 1998:14(3):202–11. https://doi.org/10.1016/S0109-5641(98)00033-5
[7] Azizi S. N., Ehsani Tilami S. Cu-modified analcime as a catalyst for oxidation of benzyl alcohol: Experimental and theoretical. *Microporous Mesoporous Materials* 2013:167:89–93. https://doi.org/10.1016/j.micromeso.2012.03.034
[8] Shah R. K. Facile synthesis of novel NiS-Analcime composite for the efficient photocatalytic degradation of Eriochrome Black T dye. *Int J Environ Anal Chem* 2020:102(19):8331–8345. https://doi.org/10.1080/03067319.2020.1849652
[9] Dyer A., Tangkawanit S., Rangsriwatananon K. Exchange diffusion of Cu^{2+}, Ni^{2+}, Pb^{2+} and Zn^{2+} into analcime synthesized from perlite. *Microporous Mesoporous Materials* 2004:75(3):273–279. https://doi.org/10.1016/j.micromeso.2004.07.007

[10] Ehsani Tilami S., Naser Azizi S. Methionine templated analcime for enhancing heavy metal adsorption. *Science Asia* 2017:43(1):42–46. https://doi.org/10.2306/scienceasia1513-1874.2017.43.042
[11] Atta A. Y., Jibril B. Y., Aderemi B. O., Adefila S. S. Preparation of analcime from local kaolin and rice husk ash. *Appl Clay Sci* 2012:61:8–13. https://doi.org/10.1016/j.clay.2012.02.018
[12] Yuan J., Yang J., Ma H., Liu C., Zhao C. Hydrothermal synthesis of analcime and hydroxycancrinite from K-feldspar in Na_2 SiO_3 solution: characterization and reaction mechanism. *RSC Adv* 2016:59:54503–54509. https://doi.org/10.1039/C6RA08080D
[13] http://www.iza-structure.org/databases/, accessed on January 7, 2024
[14] Maldonado M., Oleksiak M. D., Chinta S., Rimer J. D. Controlling Crystal Polymorphism in Organic-Free Synthesis of Na-Zeolites. *J Am Chem Soc* 2013:135(7):2641–2652. https://doi.org/10.1021/ja3105939
[15] Sobuś N., Czekaj I., Diichuk V., Kobasa I. M. Characteristics of the structure of natural zeolites and their potential application in catalysis and adsorption processes. *Tech Trans* 2020:117:1–20. https://doi.org/10.37705/TechTrans/e2020043
[16] Đặng T-H., Nguyễn X-H., Chou C-L., Chen B-H. Preparation of cancrinite-type zeolite from diatomaceous earth as transesterification catalysts for biodiesel production. *Renew Energy* 2021:174:347–358. https://doi.org/10.1016/j.renene.2021.04.068
[17] Simbi I., Osagie Aigbe U., Oyekanmi Oyekola O., Adelaja Osibote O. Chemical and quality performance of biodiesel and petrol blends. *Energy Convers Manag X* 2022:15:100256. https://doi.org/10.1016/j.ecmx.2022.100256
[18] Sakthivel R., Ramesh K., Purnachandran R., Mohamed Shameer P. A review on the properties, performance and emission aspects of the third generation biodiesels. *Renew Sustain Energy Rev* 2018:82(P3):2970–2992. https://doi.org/10.1016/j.rser.2017.10.037
[19] Rizwanul Fattah I. M., Ong H. C., Mahlia T. M. I., Mofijur M., Silitonga A. S., Rahman S. M. A., Ahmad A. State of the Art of Catalysts for Biodiesel Production. *Front Energy Res* 2020:8. https://doi.org/10.3389/fenrg.2020.00101
[20] Aleman-Ramirez J. L., Okoye P. U., Torres-Arellano S., Paraguay-Delgado F., Mejía-López M., Moreira J., Sebastian P. J. Development of reusable composite eggshell-moringa leaf catalyst for biodiesel production. *Fuel* 2022:324(PB):124601. https://doi.org/10.1016/j.fuel.2022.124601
[21] Doyle A. M., Albayati T. M., Abbas A. S., Alismaeel Z. T. Biodiesel production by esterification of oleic acid over zeolite Y prepared from kaolin. *Renew Energy* 2016:97:19–23. https://doi.org/10.1016/j.renene.2016.05.067
[22] Wdowin M., Franus M., Panek R., Badura L., Franus W. The conversion technology of fly ash into zeolites. *Clean Technol Environ Policy* 2014:16:1217–1223. https://doi.org/10.1007/s10098-014-0719-6
[23] Panek R., Madej J., Bandura L., Słowik G. Recycling of Waste Solution after Hydrothermal Conversion of Fly Ash on a Semi-Technical Scale for Zeolite Synthesis. *Materials (Basel)* 2021:14(6):1413. https://doi.org/10.3390/ma14061413
[24] Grabias-Blicharz E., Panek R., Franus M., Franus W. Mechanochemically Assisted Coal Fly Ash Conversion into Zeolite. *Materials (Basel)* 2022:15(20):7174. https://doi.org/10.3390/ma15207174
[25] Jamil T. S., Youssef H. F. Microwave synthesis of zeolites from Egyptian kaolin: Evaluation of heavy metals removal. *Sep Sci Technol* 2016:51(18):2876–2886. https://doi.org/10.1080/01496395.2016.1229337
[26] Hegazy E. Z., El Maksod I. H. A., El Enin R. M. M. A. Preparation and characterization of Ti and V modified analcime from local kaolin. *Appl Clay Sci* 2010:49(3):149–155. https://doi.org/10.1016/j.clay.2010.04.019
[27] Bandura L., Panek R., Madej J., Franus W. Synthesis of zeolite-carbon composites using high-carbon fly ash and their adsorption abilities towards petroleum substances. *Fuel* 2021:283:119173. https://doi.org/10.1016/j.fuel.2020.119173
[28] Zinatlou Ajabshir S., Gucuyener C., Vivacqua V., Gobby D., Stitt H., Barletta D., *et al.* Flow behaviour of zeolite powders at high process temperatures. *Powder Technol* 2022:409:117818. https://doi.org/10.1016/j.powtec.2022.117818
[29] Zhang X., Tang D., Zhang M., Yang R. Synthesis of NaX zeolite: Influence of crystallization time, temperature and batch molar ratio SiO_2/Al_2O_3 on the particulate properties of zeolite crystals. *Powder Technol* 2013:235:322–8. https://doi.org/10.1016/j.powtec.2012.10.046
[30] Purandaradas A., Silambarasan T., Murugan K., Babujanarthanam R., Gandhi A. D., Dhandapani K. V., Anbumani D., Kavitha P. Development and quantification of biodiesel production from chicken feather meal as a cost-effective feedstock by using green technology. *Biochem Biophys Reports* 2018:14:133–139. https://doi.org/10.1016/j.bbrep.2018.04.012
[31] Primo A., Garcia H. Zeolites as catalysts in oil refining. *Chem Soc Rev* 2014:22:7548–7561. https://doi.org/10.1039/C3CS60394F
[32] Blanco C., González F., Pesquera C., Benito I., Mendioroz S., Pajares J. A. Differences Between One Aluminic Palygorskite and Another Magnesic by Infrared Spectroscopy. *Spectrosc Lett* 1989:22(6):659–673. https://doi.org/10.1080/00387018908053926

[33] Kwakye-Awuah B., Radecka I., Kenward M. A., Williams C. D. Production of silver-doped analcime by isomorphous substitution technique. *J Chem Technol Biotechnol* 2008:83(9):1255–1260. https://doi.org/10.1002/jctb.1938

[34] Liu X., Wang C., Zhou J., Liu C., Liu Z., Shi J., Wang Y., Teng J., Xie Z. Molecular transport in zeolite catalysts: depicting an integrated picture from macroscopic to microscopic scales. *Chem Soc Rev* 2022:51(19):8174–8200. https://doi.org/10.1039/D2CS00079B

[35] Cuautli C., Romero-Ibarra I., Vazquez-Arenas J., Galvan M. Determination of active sites on Na_2SiO_3 and Li_2SiO_3 catalysts for methanol dissociation and methoxide stabilization concerning biodiesel production. *Fuel* 2021:298:120840. https://doi.org/10.1016/j.fuel.2021.120840

[36] Kouzu M., Kasuno T., Tajika M., Sugimoto Y., Yamanaka S., Hidaka J. Calcium oxide as a solid base catalyst for transesterification of soybean oil and its application to biodiesel production. *Fuel* 2008:87(12):2798–28806. https://doi.org/10.1016/j.fuel.2007.10.019

[37] Al-Jammal N., Al-Hamamre Z., Alnaief M. Manufacturing of zeolite based catalyst from zeolite tuft for biodiesel production from waste sunflower oil. *Renew Energy* 2016:93:449–459. https://doi.org/10.1016/j.renene.2016.03.018

[38] Fereidooni L., Abbaspourrad A., Enayati M. Electrolytic transesterification of waste frying oil using Na+/zeolite–chitosan biocomposite for biodiesel production. *Waste Manag* 2021:127:48–62. https://doi.org/10.1016/j.wasman.2021.04.020

[39] Enweremadu C., Samuel O., Rutto H. Experimental Studies and Theoretical Modelling of Diesel Engine Running on Biodiesels from South African Sunflower and Canola Oils *Environ Clim Technol* 2022:26:630–647. https://doi.org/10.2478/rtuect-2022-0048

[40] Kiprono J, Rutto H, Seodigeng T. Production of Biodiesel Using Phosphate Rock as a Heterogeneous Catalyst. An Optimized Process Using Surface Response Methodology *Environ Clim Technol* 2022:26:822–835. https://doi.org/10.2478/rtuect-2022-0062

[41] Rashid A.B, Kader M.F. Performance Analysis of An Automated Biodiesel Processor *Environ Clim Technol* 2022:26:84–97. https://doi.org/10.2478/rtuect-2022-0008

ANNEX

TABLE S1. PERCENTAGE SHARE (%) OF GRAIN FRACTIONS OF ANALCIME ZEOLITES

Fraction, µm	ANA1	ANA2	ANA3	HIC-ANA
	Volume, %			
0.01–2 µm	0.57	0.13	2.81	1.87
2–20 µm	19.49	17.85	31.25	17.13
20–50 µm	15.05	34.45	26.33	34.57
50–100 µm	18.06	26.22	19.89	35.56
100–250 µm	32.70	15.81	16.04	10.29
250–500 µm	13.69	3.47	3.66	0.58
500–1000 µm	0.43	1.48	0.02	–
1000–2000 µm	–	0.50	–	–

TABLE S2. PERCENTILES – D10, D50, D90- SHARE (MM) OF GRAIN FRACTIONS OF ANALCIME ZEOLITES AND HIC-ANA

	ANA1	ANA2	ANA3	HIC-ANA
Dx (10)	10.8 µm	13.3 µm	4.83 µm	9.43 µm
Dx (50)	90.4 µm	47.3 µm	35.7 µm	47.2 µm
Dx (90)	285 µm	169 µm	161 µm	103 µm

TABLE S3. CRYSTALLINITY QUANTITATIVE CONTENT

Crystallinity quantitative, %	Sample
100	ANA3
93	ANA1
94	ANA2
49	HIC-ANA

TABLE S4. RESULTS OF GC-MS CHEMICAL ANALYSIS OF USED COOKING OIL

Compound	Quantity in used cooking oil
Dodecanoic acid	5.2
Hexadecanoic acid	12.7
9,12-Octadecanoic acid	24.7
9-Octadecanoic acid	39.4
Octadecanoic acid	15.5
9,12,15-Octadecatrienoic acid	2.1
Eicosanoic acid	0.4

TABLE S5. RESULTS OF GC-MS ANALYSIS OF BIODIESEL CONTENT WITH ANA3 USED AS THE CATALYST, ACHIEVED UNDERNEATH OPTIMAL REACTION CIRCUMSTANCES

Compound	Composition of biodiesel 230 °C, %
Dodecanoic acid, methyl ester	1.2
Hexadecanoic acid, methyl ester	15.8
9,12-Octadecadienoic acid, methyl ester	24.9
9-Octadecenoic acid, methyl ester	49.2
Octadecanoic acid, methyl ester	5.2
9,15-Octadecadienoic acid, methyl ester	3.4
Eicosadienoic acid, methyl ester	0.3

TABLE S6. BIODIESEL YIELD

Biodiesel yield	ANA1	ANA2	ANA3	HIC-ANA
			%	
180 °C	87.2	85.1	89.1	82.0
230 °C	94.5	95.2	97.2	88.7

TABLE S7. RESULTS OF BIODIESEL PARAMETERS WITH ANA3 CATALYST

Parameter	Crude cooking oil	Biodiesel 180	Biodiesel 230
Density at 15 °C, kg/m^3	974	872	869
Viscosity, mm^2/s	30.192	4.671	4.974